Title: Subjective cognitive decline predicts lower cingulo-opercular network functional connectivity in individuals with lower neurite density in the forceps minor

Author names and affiliations: Adriana L. Ruiz-Rizzo [a], Raymond P. Viviano [b], Ana M. Daugherty [b], Kathrin Finke [c], Hermann J. Müller [a], Jessica S. Damoiseaux [b]

[a] Department of Psychology, General and Experimental Psychology Unit, LMU Munich, Munich, 80802, Germany

[b] Department of Psychology, Institute of Gerontology, Wayne State University, Detroit, MI, 48202, U.S.A.

[c] Hans-Berger Department of Neurology, Jena University Hospital, Jena, 07747, Germany

Corresponding author: Adriana L. Ruiz-Rizzo: adriana.ruiz@lmu.de, Department of Psychology, Ludwig-Maximilians-Universität Mu□nchen, Leopoldstr. 13, 80802 Munich, Germany

Running head: Cingulo-opercular network in SCD

Abbreviations: BOLD: blood oxygenation level-dependent signal; CON-FC: cingulo-opercular network functional connectivity; CON-SC: cingulo-opercular network structural connectivity; fMRI: functional magnetic resonance imaging; LGCM: Latent growth curve modeling; MFQ: memory functioning questionnaire; NODDI: Orientation Dispersion and Density Imaging; SCD: subjective cognitive decline

Abstract

Cognitive complaints of attention/concentration problems are highly frequent in older adults with subjective cognitive decline (SCD). Functional connectivity in the cingulo-opercular network (CON-FC) supports cognitive control, tonic alertness, and visual processing speed. Thus, those complaints in SCD may reflect a decrease in CON-FC. Frontal white-matter tracts such as the forceps minor exhibit age- and SCD-related alterations and, therefore, might influence the CON-FC decrease in SCD. Here, we aimed to determine whether SCD predicts an impairment in CON-FC and whether neurite density in the forceps minor modulates that effect. To do so, we integrated cross-sectional and longitudinal analyses of multimodal data in a latent growth curve modeling approach. Sixty-nine healthy older adults (13 males; 68.33 ± 7.95 years old) underwent resting-state functional and diffusion-weighted magnetic resonance imaging, and the degree of SCD was assessed at baseline with the memory functioning questionnaire (greater score indicating more SCD). Forty-nine of the participants were further enrolled in two follow-ups, each about 18 months apart. Baseline SCD did not predict CON-FC after three years or its rate of change (p-values > 0.092). Notably, however, the forceps minor neurite density did modulate the relation between SCD and CON-FC (intercept; b = 0.20, 95% confidence interval, CI, [0.03, 0.37], p = 0.020), so that SCD predicted a greater CON-FC decrease in older adults with relatively lower neurite density in the forceps minor. The neurite density of the forceps minor, in turn, negatively correlated with age. These results suggest that CON-FC alterations in SCD are dependent upon the forceps minor neurite density. Moreover, these results imply modifiable age-related factors that could help delay or mitigate both age and SCD-related effects on brain connectivity.

Keywords: functional connectivity; latent growth curve modeling; neurite density; salience network; subjective cognitive decline

Introduction

Subjective cognitive decline (SCD) is the perceived worsening of cognitive abilities, unrelated to an acute event and characterized by normal performance in standard neuropsychological tests (Molinuevo et al., 2017). SCD is associated with changes in the functional connectivity (FC – or the observed correlations between distant regions) (Friston, 1994) within and between the default mode network and medial temporal lobe regions (Viviano & Damoiseaux, 2020). Less is known about SCD-related differences in other potentially relevant networks such as the 'cingulo-opercular' network (CON), in which FC decreases in aging and mild cognitive impairment (He et al., 2014). CON-FC supports cognitive control, tonic alertness, and visual processing speed (Dosenbach et al., 2007; Ruiz-Rizzo et al., 2018; Sadaghiani & Kleinschmidt, 2016) that are all vulnerable to decline in aging (e.g., McAvinue et al., 2012; Ruiz-Rizzo et al., 2019). As cognitive complaints related to attention/concentration problems are highly frequent in older adults with SCD (La Joie et al., 2016; Valech et al., 2018), CON-FC might also be associated with SCD. Furthermore, the pattern of observed differences in FC has been proposed to vary according to the time since SCD onset (e.g., increases at the start of SCD and decreases if approaching a mild cognitive impairment stage; Viviano & Damoiseaux, 2020). Accordingly, only with a longitudinal approach can we set an individual's putative SCD onset and baseline FC. Then, FC changes can more clearly be determined. In the present study, we evaluated SCD-related differences in CON-FC integrating both cross-sectional and longitudinal analyses in a latent growth curve modeling approach.

Although strong FC can exist between brain regions with no direct white matter connection, structural connections do constrain and provide a 'physical substrate' to FC (Honey et al., 2009; Raichle, 2015; Z. Wang et al., 2015). Thus, the white matter in

tracts connecting some of the CON regions (i.e., structural connectivity, SC – or the modeled diffusion direction of water molecules; Assaf et al., 2019) might modulate the magnitude of SCD-related differences in CON-FC. Particularly for CON, FC-guided tractography has shown that its SC mainly connects the anterior cingulate cortex with other CON regions (e.g., middle frontal gyrus, anterior insula; Figley et al., 2015). Both reduced CON-SC (i.e., lower fractional anisotropy; Figley et al., 2015) and CON-FC (e.g., Onoda et al., 2012; Ruiz-Rizzo et al., 2019) are observed with more advanced age. The forceps minor, a major commissural tract formed from the projections from the genu of the corpus callosum (Wakana et al., 2004), connects the medial (i.e., anterior cingulate cortex) and lateral surfaces of the frontal lobes and can be identified in humans in vivo with diffusion-weighted imaging (Abe et al., 2004). Thus, we studied the forceps minor as a proxy of CON-SC for two main reasons. First, it is a major structural pathway in the CON and, second, its diffusion properties can be measured in vivo.

The particular relevance of the forceps minor white matter in SCD is illustrated by a recent study which reported that fractional anisotropy and mean diffusivity of the forceps minor exhibit alterations in SCD and mild cognitive impairment (e.g., Luo et al., 2020). In addition, lower fractional anisotropy and higher mean diffusivity of commissural tracts, including the forceps minor, have been observed with increasing age (de Groot et al., 2015). The degree of fractional anisotropy in the forceps minor relates to performance in executive function (Ohlhauser et al., 2019) and visual attention (Tu et al., 2018) tasks in SCD and/or mild cognitive impairment – i.e., cognitive functions in which complaints are frequent in SCD (Valech et al., 2018). Lastly, in carriers of autosomal Alzheimer's disease mutations, increased mean diffusivity in the forceps minor appears to precede symptom onset (Araque Caballero et al., 2018). Accordingly, we hypothesized that individual differences in diffusion

metrics of the forceps minor modify the relationship between SCD and CON-FC. We focused on the neurite density of the forceps minor, in particular, because neurite density has been proposed to be a more sensitive marker of pathology than other white matter diffusion metrics (e.g., fractional anisotropy) (Zhang et al., 2012).

In the present study, we aimed to evaluate SCD-related differences in CON-FC and whether CON-SC modulates that effect, by using longitudinal, multimodal data. More specifically, we analyzed CON-FC and CON-SC across three time points, ~ 18 months apart, in a sample of healthy older adults in which the degree of SCD was quantified at baseline. We used latent growth curve modeling to test the following two hypotheses: (i) baseline SCD predicts a decrease in CON-FC over three years, and (ii) the decrease in CON-FC is more pronounced in older adults with relatively lower CON-SC as obtained from the neurite density in the forceps minor.

Materials and Method

Participants

Sixty-nine healthy older participants (13 males; mean age: 68.33 ± 7.95 years; age range: 50 - 85 years; 78% self-identified as Black) underwent neuropsychological testing and resting-state functional and diffusion-weighted magnetic resonance imaging (MRI) at baseline. Participants were volunteers recruited from the community of Metro Detroit (MI, USA). Forty-nine of those 69 participants were enrolled in a longitudinal study, which consisted of two follow-ups, each approximately 18 months apart (mean: 18.5 ± 1.39 months). Thirty-four (69%) of the 49 participants returned for the first follow-up and 29 (55%) for the second follow-up. CON-SC data were missing for 8 participants at baseline and 1 participant at the last follow-up, and MFQ was missing for 1 participant at baseline. Little's MCAR test was not significant (χ^2 (108, N = 69) = 100, p = 0.690, missing patterns = 9), supporting the conclusion that data were

missing at random. All participants were right-handed and fulfilled the selection criteria, including no recent or past history of psychiatric disorders, neurological disease, or head trauma, no current use of psychoactive medication, and no contraindications for MRI. The Institutional Review Board of Wayne State University approved all the procedures used in this study, which followed the ethical principles of the World Medical Association Declaration of Helsinki. All participants gave written informed consent before their participation in the study. Demographic data for each measurement occasion are listed in Table 1. The longitudinal functional MRI and the baseline diffusion-weighted MRI data used in the current study have been reported previously (Viviano et al., 2019; Viviano & Damoiseaux, 2021).

Table 1. Demographic variables across the three time points.

Variable	**Baseline** (*n* = 69)	**Follow-up 1** (*n* = 34)	**Follow-up 2** (*n* = 29)
Age at baseline	68.33 ± 7.95	67.41 ± 8.95	66.28 ± 9.40
Sex [*n* (%)] F / M	56 (81.2%) / 13 (18.8%)	29 (85.3%) / 5 (14.7%)	19 (65.5%) / 10 (34.5%)
Education level			
High school	24 (35.3%)	12 (38.7%)	11 (40.7%)
Associate degree	18 (26.5%)	7 (22.6%)	5 (18.6%)
University	26 (38.2%)[a]	12 (38.7%)[c]	11 (40.7%)[b]
Family history of dementia (yes / no)	34 (50.7%) / 33 (49.3%)[b]	19 (55.9%) / 15 (44.1%)	11 (39.3%) / 17 (60.7%)[a]
Time since previous measurement (months)	–	18.62 ± 1.17	17.13 ± 5.10[a]

Number of missing data points = [a] 1, [b] 2, [c] 3

SCD, behavioral, and neuropsychological measures

SCD was quantified with the General Frequency of Forgetting factor of the Memory Functioning Questionnaire (MFQ; Gilewski et al., 1990). These scores were inverted[1] to obtain a more intuitive interpretation of them, with higher scores indicating a greater degree of SCD. Depressive symptoms were measured with the Geriatric Depression Scale (Yesavage et al., 1982), and the Big Five Inventory (John et al., 1991) was used to measure personality traits of neuroticism and conscientiousness. Global cognition was assessed through the Mini-Mental State Examination (MMSE; Folstein et al., 1975) and the Wechsler Abbreviated Scale of Intelligence II (Wechsler, 2011). To assess attention, we used the Trail Making Test (TMT; Reitan & Wolfson, 1986), part A, and the digit symbol-coding subtest of the Wechsler Adult Intelligence Scale III (Wechsler, 1997). The Rey Auditory Verbal Learning Task (Rey, 1958) and the adult battery of the Wechsler Memory Scale-IV (Wechsler, 2009) were used to assess memory. Executive function measures were obtained through the TMT, part B, and the Stroop test (Stroop, 1935). Finally, a measure of language was obtained through a semantic fluency task (animals and occupations). Average group performance in all neuropsychological measures is presented in Table 2, separately for each measurement occasion. To evaluate measurement invariance in neuropsychological assessments across study occasions and SCD, linear mixed-effects models were fitted to the data using the *lme4* package in R (v. 4.1.0; R Core Team, 2021; RStudio Team, 2021; https://www.R-project.org/). Model parameters were assessed by 95% confidence intervals (CI), which if not overlapping zero support interpretation of the effect size.

[1] For each response x of the 33 factor items: $(8 - x) / 33$.

Table 2. SCD, behavioral, and neuropsychological measures across the three time points

Variable	**Baseline** (*n* = 69) Mean ± SD	**18-mos Follow-up** (*n* = 34) Mean ± SD	**36-mos Follow-up** (*n* = 29) Mean ± SD
SCD			
MFQ - General Frequency of Forgetting	2.99 ± 0.91[a]	2.95 ± 0.95[a]	2.91 ± 0.79[a]
Behavioral			
Geriatric Depression Scale	3.82 ± 3.93[b]	3.62 ± 3.70	3.71 ± 3.71[a]
Big Five Inventory – Conscientiousness	37.36 ± 5.49[c]	37.35 ± 4.61[c]	36.75 ± 4.57[a]
Big Five Inventory – Neuroticism	17.41 ± 6.00[c]	17.29 ± 5.39[c]	17.89 ± 5.74[a]
Global cognition			
Mini-Mental State Examination	28.33 ± 1.97[b]	28.84 ± 1.16[c]	28.86 ± 1.30[a]
General IQ	98.09 ± 11.45[a]	101.87 ± 12.93[c]	100.96 ± 13.03[a]
Attention			
Trail Making Test A [time (s)]	47.43 ± 21.00[e]	50.01 ± 31.53[c]	55.77 ± 32.29[a]
Digit Symbol Substitution (total score)	39.78 ± 11.41[d]	41.71 ± 10.89[c]	43.86 ± 13.06[a]
Memory			
Rey Auditory Verbal Learning (total)	46.43 ± 9.31[b]	48.90 ± 8.87[d]	47.64 ± 10.03[a]
WMS Auditory Memory Index	0.47 ± 0.12[c]	0.55 ± 0.11[c]	0.54 ± 0.13[a]
WMS Visual Memory Index	0.54 ± 0.11[f]	0.55 ± 0.12[c]	0.57 ± 0.15[a]
WMS Visual Working Memory Index	0.40 ± 0.12[d]	0.42 ± 0.11[d]	0.41 ± 0.15[a]
WMS Immediate Memory Index	0.55 ± 0.10[f]	0.58 ± 0.10[c]	0.58 ± 0.12[a]
WMS Delayed Memory Index	0.47 ± 0.11[e]	0.51 ± 0.12[c]	0.53 ± 0.14[a]
Executive Function			
Trail Making Test B [time (s)]	124.18 ± 82.67[d]	103.51 ± 59.62[c]	109.91 ± 67.67[a]
Stroop Test Ratio Score	1.98 ± 0.45[g]	1.87 ± 0.26[h]	2.00 ± 0.41[g]
Language			
Verbal Fluency (total score)	36.55 ± 7.46[d]	39.74 ± 7.82[c]	38.04 ± 8.79[a]

Number of missing data points = [a] 1, [b] 2, [c] 3, [d] 4, [e] 5, [f] 6, [g] 7, [h] 8

MRI data acquisition

Structural MRI data were acquired on a Siemens Magnetom Verio 3-Tesla scanner (Siemens Healthcare, Erlangen, Germany) located at the Wayne State University MR Research Facility (Detroit MI, United States), using a 32-channel Head Matrix coil. A high-resolution anatomical image was obtained through a T1-weighted 3D magnetization-prepared rapid gradient-echo (MP-RAGE) sequence, with the following parameters: 176 slices parallel to the bicommissural line, slice thickness = 1.3 mm, repetition time (TR) = 1680 ms, echo time (TE) = 3.51 ms, inversion time = 900 ms, flip angle = 9°, bandwidth = 180 Hz/pixel, GRAPPA acceleration factor = 2, field of view (FOV) = 256 mm, matrix size = 384 × 384, and voxel size = 0.7 × 0.7 × 1.3 mm.

Diffusion-weighted MRI data were acquired through a multiband (acceleration factor = 3) echo-planar imaging (EPI) sequence, with the following parameters: 84 axial slices, slice thickness = 2 mm, TR = 3500 ms, TE = 87 ms, flip angle = 90°, refocus flip angle = 160°, bandwidth = 1724 Hz/pixel, GRAPPA acceleration factor = 2, FOV = 200 mm, matrix size = 100 × 100, voxel size = 2.00 mm isotropic, phase encoding = anterior to posterior, diffusion directions = 96 (6 without diffusion weighting, b = 0), b-values = 1000 (30 directions) & 1800 (60 directions) s/mm^2, total time of acquisition (TA) = 6 min 1 s.

Resting-state functional MRI data were acquired through a high-resolution multiband (acceleration factor = 3) T2*-weighted EPI sequence, with the following parameters: 75 slices, slice thickness = 2 mm, TR = 2000 ms, TE = 30 ms, flip angle = 73°, bandwidth = 1698 Hz/pixel, GRAPPA acceleration factor = 2, FOV = 256 mm, matrix size = 128 × 128, voxel size = 2 mm isotropic, phase encoding = anterior to

posterior, 220 volumes, TA = 7 min 36 s. Participants were asked to remain with their eyes closed during the resting-state functional MRI procedure.

A field map for susceptibility-derived distortion correction was acquired through two multiband (acceleration factor = 3) spin-echo echo-planar images of opposing phase encoding directions (anterior to posterior and posterior to anterior), with the following parameters: 75 slices, slice thickness = 2 mm, TR = 2412 ms, TE = 51 ms, flip angle = 90°, refocus flip angle = 180°, bandwidth = 1698 Hz/pixel, GRAPPA acceleration factor = 2, FOV = 256 mm, matrix size = 128 × 128, and voxel size = 2 mm isotropic.

Diffusion-weighted MRI data preprocessing

Prior to preprocessing, the high-resolution, T1-weighted images were anatomically segmented with Freesurfer (v.6.0; Fischl, 2012) (http://surfer.nmr.mgh.harvard.edu/). Preprocessing of diffusion-weighted MRI data was done using the TRActs Constrained by UnderLying Anatomy (TRACULA; https://surfer.nmr.mgh.harvard.edu/fswiki/Tracula) tool (Yendiki et al., 2011) in Freesurfer. Preprocessing included eddy-current distortion based on FMRIB Software Library (FSL) tools (v.5.0.8; Jenkinson et al., 2012) (https://fsl.fmrib.ox.ac.uk) and head motion correction by registering the diffusion-weighted to the b = 0 images. Next, the b = 0 image was registered to the high-resolution, T1-weighted image by an affine registration method and, subsequently, to the Montreal Neurological Institute (MNI) standard space. Finally, the anatomical priors for white-matter tracts were computed by incorporating prior knowledge on the pathways from a set of training subjects (Yendiki et al., 2011). All ensuing analyses of these data were conducted in participants' native (i.e., diffusion-weighted) space.

Resting-state fMRI data preprocessing

Resting-state fMRI data were preprocessed as described in Viviano & Damoiseaux (2021). Briefly, preprocessing was conducted using FSL FEAT (Woolrich et al., 2001) (https://fsl.fmrib.ox.ac.uk/fsl/fslwiki/FEAT), and included removal of the first five volumes, head motion correction (Jenkinson et al., 2002), removal of non-brain structures (Smith, 2002), susceptibility-derived distortion correction (Smith et al., 2004), co-registration to the anatomical image and, subsequently, to the MNI 2-mm standard space, spatial smoothing (4-mm full width at half maximum), and 4D grand-mean scaling. ICA-AROMA (Pruim et al., 2015) was used to detect and regress motion artifacts. Finally, the global signal was regressed out from the resting-state functional MRI data.

Connectivity analysis

Structural connectivity

Major white-matter tracts were automatically reconstructed and labeled in participants' native space using TRACULA, an automated Bayesian global tractography algorithm (Yendiki et al., 2011). TRACULA uses the "ball-and-stick" model of diffusion (Behrens et al., 2007) and anatomical priors for tract reconstruction, both of which yield a posterior probability for each tract given the diffusion-weighted MRI data (Yendiki et al., 2011). More specifically, FSL's bedpostX (Bayesian Estimation of Diffusion Parameters Obtained using Sampling Techniques) was used to fit the ball-and-stick model to the diffusion-weighted MRI data at every voxel. Next, the probability distributions were generated for each participant and each tract by fitting the shape of each pathway to the results of the ball-and-stick model of diffusion and to the prior knowledge of the pathway anatomy obtained from the manually annotated set of training subjects in the TRACULA atlas (Yendiki et al., 2011).

The posterior probability distribution map for the forceps minor (thresholded to 0.20 of the maximum probability value – default settings) was used as a region of interest (ROI) to obtain its average neurite density. To do so, we used the Neurite Orientation Dispersion and Density Imaging (NODDI) method (Zhang et al., 2012), as implemented in the AMICO (Accelerated Microstructure Imaging via Convex Optimization) python module (Daducci et al., 2015). NODDI follows a tissue model of three microstructural compartments that affect water diffusion differently: intracellular (space bounded by neurite membranes), extracellular (space around the neurites), and CSF (space occupied by cerebrospinal fluid) (Zhang et al., 2012). Neurite density refers to the volume fraction of the intracellular compartment and might be a sensitive marker of pathology (Zhang et al., 2012). After obtaining the voxelwise neurite density map for each participant, the mean neurite density was computed for the forceps minor. The mean neurite density was weighted by each voxel's posterior probability of tract membership (as in Viviano et al., 2019): voxels towards the center had greater posterior probabilities and voxels farther from the center had lower posterior probabilities. Thus, voxels closer to the boundary of white and gray matter contributed less to the weighted mean. Such an approach reduces the possible contribution of partial volume effects to the results. We used the mean neurite density of the forceps minor as a measure of CON-SC in the present study. A separate mean neurite density was obtained for each time point. These values were then averaged to form a single measure of CON-SC for the latent growth curve modeling analysis to reduce model complexity and the number of parameters to be estimated given our sample size.

Functional connectivity

We selected five ROIs of the CON, namely, the anterior cingulate cortex (ACC), left and right anterior insula, and left and right middle frontal gyrus, and obtained the

average time course of each ROI using FSL's *fslmeants* command (also see *Supplementary Material*). These ROIs were taken from a parcellation of the human cerebral cortex that combined information from sharp changes in architecture, function, connectivity, and topography (Glasser et al., 2016). More specifically, each of these ROIs was composed of several multimodal areas (Table 3). These areas were selected based on the descriptions presented in the supplementary neuroanatomical results of Glasser et al. (2016). To create the ROIs for the present study, the selected multimodal areas in MNI space were first extracted from the original map of 360 areas [https://github.com/brainspaces/glasser360/blob/master/glasser360MNI.nii.gz] and binarized (as all voxels had as intensity value the area number). Next, the selected areas were added together, resampled from 1-mm to 2-mm-isotropic voxel-size (i.e., the functional images' voxel size), thresholded (cutoff = 0.3), and binarized. Finally, we extracted the time courses of each ROI by first reslicing each ROI to each participant's functional space, which gave each voxel of the ROI a different value depending on the warping. Then, a weighted mean time course was computed across all voxels of the ROI, using the ROI voxels' values (range: 0 – 1) as weights. ROIs' time courses were obtained for each participant, separately per time point. Pearson's correlation was first computed between the five ROI's time series (i.e., 10 pairs), and the *r*-values were then Fisher's *r*-to-*z* transformed. Finally, the mean CON-FC was calculated from the *z*-values across the 10 ROI pairs.

Table 3. Multimodal areas comprising the CON-FC ROIs

Region	Areas	CON ROI
19 "Anterior Cingulate and Medial Prefrontal Cortex"	RH: 60, 62, 179 LH: 240, 242, 359	ACC
12 "Insular and Frontal Opercular Cortex"	RH: 108, 112	Anterior insula

	LH: 288, 292	
22 “Dorsolateral Prefrontal Cortex”	RH: 84, 86 LH: 264, 266	Middle frontal gyrus

Region naming and area numbering correspond to that in Glasser et al. (2016). ACC: anterior cingulate cortex; LH: left hemisphere; RH: right hemisphere; ROI: region of interest.

Latent growth curve modeling

Hypotheses were tested using a latent growth curve model (LGCM; McArdle, 2009) in a longitudinal structural equation model framework. LGCMs allow estimating between-person differences in within-person patterns of change over time (Curran et al., 2010). Specifically, the means and variances of two factors across individuals can be obtained, namely, the latent intercept and the latent slope. One big advantage of LGCM within the structural equation modeling framework is that hypotheses are tested with latent variables estimated independently of the effects of measurement error in the observed variables (Bollen & Noble, 2011; Curran et al., 2010). Observed data were standardized (i.e., mean-centered and scaled by the standard deviation separately for each time point) prior to model fit. The latent intercept corresponds to the last follow-up. Accordingly, the latent slope weights used were -2, -1, and 0, for baseline, first, and second follow-up, respectively. The pattern of data missingness was examined for indications of data missing at random and further tested with Little’s (R. J. A. Little, 1988) test as implemented in the *mcar_test* function of the *naniar* package in R. Multivariate normality was verified through Henze-Zirkler’s multivariate normality test as implemented in the *MVN* R package, which also includes Anderson-Darling’s univariate normality test. The model was thus estimated with full information maximum likelihood (FIML), a method that allows all available data to be used for parameter estimation under the assumptions of data missing at random and multivariate normality (Enders & Bandalos, 2001). When assumptions are met, FIML

estimation is the recommended practice for good external validity in longitudinal analysis with attrition (e.g., Little et al., 2014). The LGCM was estimated using the 'lavaan' package (v. 0.6-9; Rosseel, 2012) (https://lavaan.ugent.be/) in R. Model parameter estimates are reported as standardized.

Longitudinal measurement invariance

Longitudinal measurement invariance was confirmed by no change in CFI and RMSEA when imposing model constraints to be equal across time points, and by non-significant results in the Chi-squared difference test between three nested measurement models that gradually increased the constraints imposed on them (see Supplementary Table S4). Multivariate (HZ = 0.84, *p*-value = 0.547) and univariate (Anderson-Darling statistic range = 0.22 – 0.69, *p*-values > 0.062) normality was confirmed for baseline age, baseline SCD, CON-FC for each time point, and CON-SC averaged across time points.

Conditional CON-FC LGCM

A conditional LGCM tested whether SCD (as indexed by the MFQ) at baseline predicts CON-FC (averaged across all CON-FC ROIs) at the last follow-up (latent intercept) and/or the rate of change towards the last follow-up of CON-FC (latent slope) (Fig. 1). Accordingly, the latent intercept of CON-FC was centered at the last time point – similar to the lead-lag approach used in Daugherty and Raz (2016). The interaction between CON-SC and SCD was included to test the moderation of CON-SC on the effect of SCD on CON-FC as a predictor of the latent intercept of CON-FC. As CON-SC was obtained by averaging across all time points, its direct effect was also included in the model, i.e., by pointing towards the latent slope of CON-FC. For completeness, an alternative model was tested in which the moderation and direct

effects of CON-SC were swapped with respect to the latent intercept and slope of CON-FC (i.e., with the moderation pointing to the slope and direct effect pointing to the intercept). Effects were considered significant at a Bonferroni-corrected α-level = 0.025 (i.e., to account for the two models tested). Age at baseline was used as a (time-invariant) control covariate, and all observed measures were centered at 0 with a standard deviation of 1.

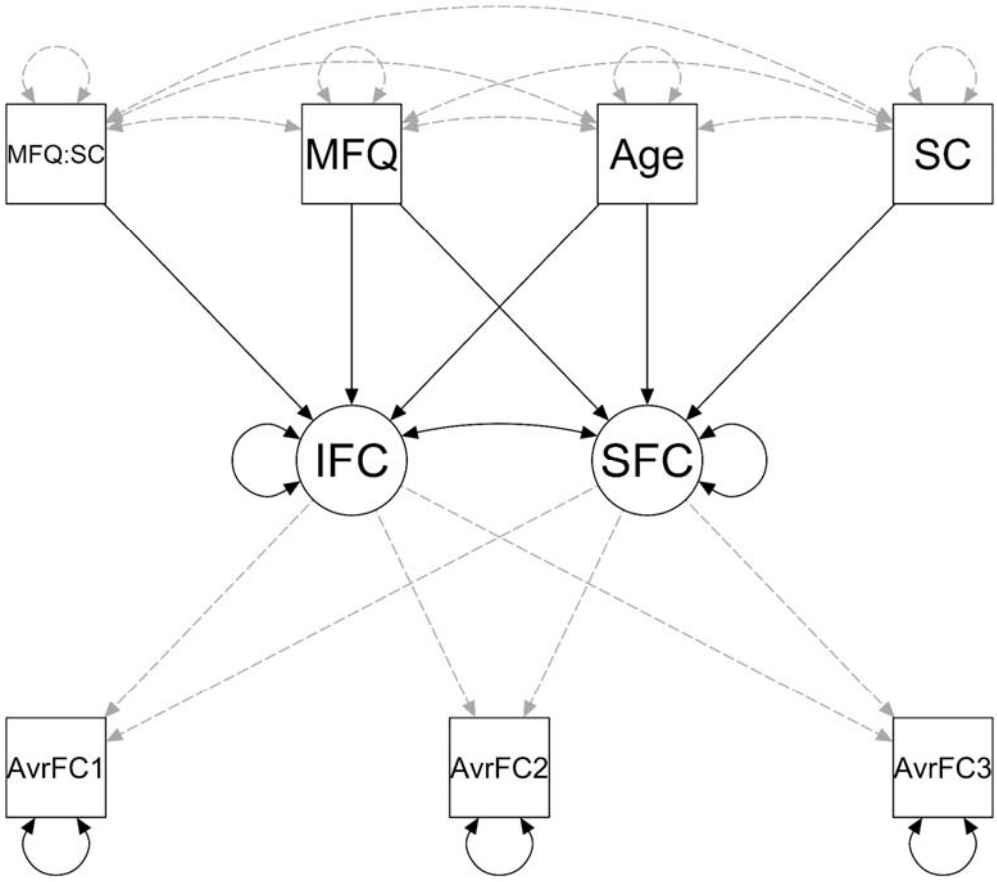

Fig 1. Conditional latent growth curve model path diagram. Model to test the effect of subjective cognitive decline, measured with the Memory Functioning Questionnaire (MFQ), on the latent intercept ('IFC') and slope ('SFC') of the functional connectivity averaged across regions of interest of the cingulo-opercular network ('AvrFC') for each measurement occasion. The model also includes the effect of structural connectivity ('SC') of the forceps minor and the interaction between MFQ and SC ('MFQ:SC'). The directional effects of 'SC' and 'MFQ:SC' were also tested on the latent intercept and slope, respectively. Exogenous or predictor variables are on the top. Black arrows indicate that the effects were estimated, whereas gray, dotted arrows indicate that the effects were fixed. Squares represent manifest variables,

while circles latent variables. Straight arrows indicate the directionality of a direct effect. Curved, double-headed arrows represent correlations or residual variances.

Model evaluation

As there is 'error' (or unexplained variance) inherently associated with the measurement required to estimate CON-FC on each occasion, we ensured good consistency of measurement across study occasions to support the validity of the latent variables. Accordingly, invariance over time was assessed in the measurement model (latent variables and their three indicators; middle and lower part of Fig. 1) and ensured in the structural model (Fig. 1) by estimating variances within a latent construct and constraining them to be equal across time (van de Schoot et al., 2012). Model fit was determined by examining the Chi-square (χ^2) statistic (a non-significant value for acceptance), the comparative fit index (CFI ≥ .95 for acceptance), the root mean square error of approximation (RMSEA < .08 for acceptance), and the standardized root mean square residual (SRMR ≤ .08 for acceptance) (Schreiber et al., 2006).

Data availability

The structured data and scripts used to generate these results are openly available and can be downloaded from https://osf.io/zaef2/.

Results

Behavioral and neuropsychological measures

All behavioral and neuropsychological measures across the three time points are listed in Table 2. Linear mixed model analyses revealed that depressive symptoms increased and conscientiousness scores decreased across time points and with higher baseline SCD (see Supplementary Tables S2 and S3). There was also a time

point × SCD interaction for both depressive symptoms and conscientiousness. For both depressive symptoms and conscientiousness, this interaction indicated a reduced association with SCD at the second follow-up. For depressive symptoms, the association became less positive with time, whereas for conscientiousness, the association became less negative with time. No other behavioral or neuropsychological measure varied across time points or with the degree of SCD. Age and SCD at baseline were not correlated (r_{68} = 0.14, 95% CI [-0.11, 0.36], p = 0.269).

CON structural and functional connectivity

The ROIs from which the respective connectivity values were extracted for the LGCM are shown in Fig. 2A (CON-SC) and Fig. 2C (CON-FC). The line plots in Fig. 2B (CON-SC) and Fig. 2D (CON-FC) further illustrate the mean and variability in those values in the present sample across time points. CON-SC (averaged across time points) was negatively correlated with age at baseline (r_{67} = -0.35, 95% CI [-0.55, -0.12], p = 0.003). CON-SC tended to correlate negatively with baseline SCD (r_{66} = -0.22, 95% CI [-0.44, 0.02], p = 0.072).

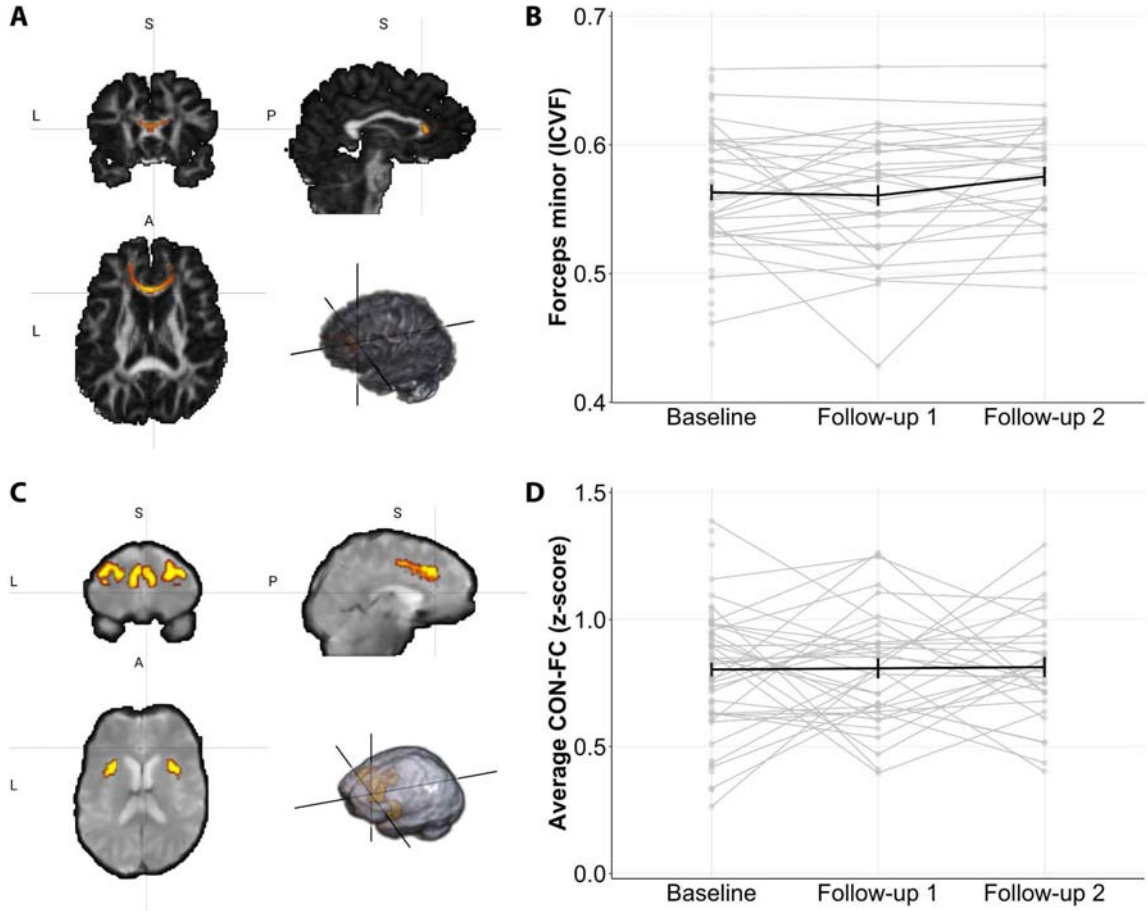

Fig 2. Individual and mean values of structural (SC) and functional (FC) connectivity of the cingulo-opercular network (CON). (A) Reconstructed forceps minor map in an exemplary participant. Neurite density (i.e., intracellular volume fraction, ICVF) values were obtained from this region of interest (ROI) for each participant and each time point as our measure of SC. (B) Individual (gray lines) and mean (black line) ICVF values of the forceps minor for each timepoint. (C) ROIs that composed the CON. To measure FC, correlations were computed between these ROIs (see Table 3) and an average was obtained for each participant and each time point. (D) Individual (gray lines) and mean (black line) FC values of the CON for each time point. The differing voxel intensity values in the ROIs were used to compute weighted averages of neurite density and time series in A and C, respectively. Error bars represent the standard errors of the respective means.

CON-SC modifies the effect of SCD on CON-FC

The conditional LGCM of CON-FC had adequate fit (χ^2 (9, n = 69) = 8.09, p = 0.525, CFI = 1.0, RMSEA = 0.0, and SRMR = 0.096). On average, SCD (as indexed by a higher MFQ) did not predict CON-FC after three years (latent intercept: β = -0.19,

Standard Error, SE = 0.15, 95% CI [-0.49, 0.11], p = 0.211) or its rate of change (latent slope: β = -0.17, SE = 0.10, 95% CI [-0.37, 0.03], p = 0.093), contrary to what was hypothesized. However, CON-SC (averaged across all time points) moderated the relation between baseline SCD and CON-FC after three years (β = 0.20, SE = 0.09, 95% CI [0.03, 0.37], p = 0.020; Fig. 3A), indicating that high baseline SCD predicts lower CON-FC after 3 years *given* a relatively low level of CON-SC throughout the 3-year time period (Fig. 3B). Neither the effect of CON-SC on the latent slope of CON-FC (95% CI [-0.18, 0.07], p = 0.406) nor the effect of age on the latent intercept (95% CI [-0.33, 0.22], p = 0.698) or slope of CON-FC (95% CI [-0.17, 0.21], p = 0.839) were significant.

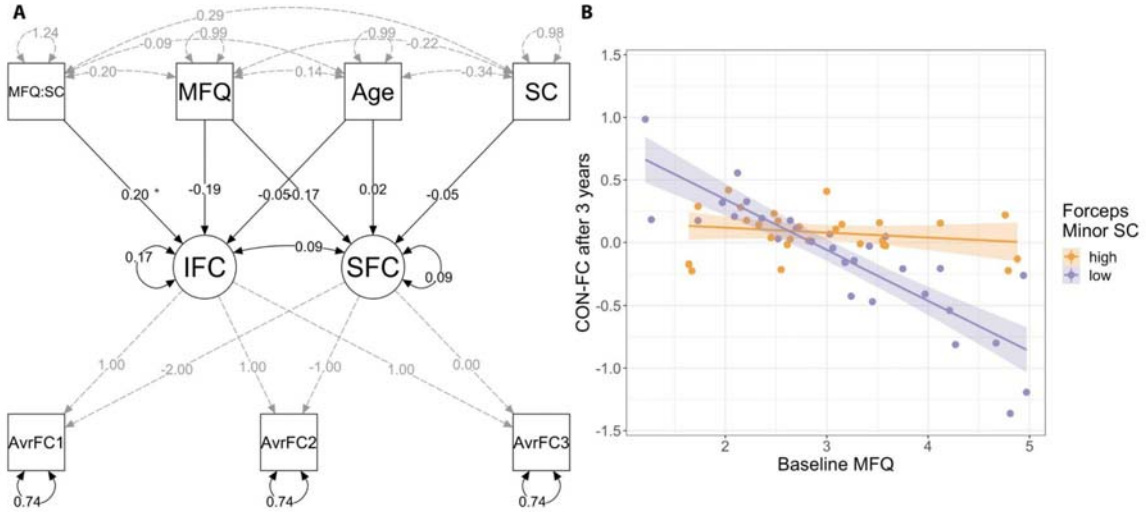

Fig 3. Conditional LGCM of CON-FC. (A) The effects of SCD (indexed by the inverted scores in the MFQ) on the latent intercept ('IFC') and slope ('SFC') of CON-FC were tested as well as the moderation of CON-SC on the relationship between MFQ and IFC (arrow from the left-most top square). The moderation effect is illustrated in (B). (B) CON-SC, represented by the forceps minor neurite density, moderated the relationship between baseline SCD and CON-FC after 3 years. Note that the division into high and low CON-SC is for illustrative purposes only; the analysis was performed using CON-SC as a continuous variable. * p < 0.025.

For completeness, an alternative model was tested in which the moderation and direct effects of CON-SC were swapped with respect to the latent intercept and

slope of CON-FC – that is, CON-SC may plausibly moderate the slope of CON-FC. The model had adequate fit (χ^2 (9, n = 69) = 6.48, p = 0.691, CFI = 1.0, RMSEA = 0.0, and SRMR = 0.080), and there was no evidence to suggest moderation; therefore, the alternative hypothesis of CON-SC on the relationship between baseline SCD and the latent slope of CON-FC was rejected (95% CI [-0.19, 0.02], p = 0.110) (see Supplementary Fig. S3). A marginal, nominally significant effect was observed for CON-SC on the latent intercept of CON-FC that did not survive family-wise error correction (β = 0.22, SE = 0.11, 95% CI [0.08, 0.44], p = 0.042, *ns* at the Bonferroni-corrected α-level). As with the previous model, neither SCD (intercept: 95% CI [-0.45, 0.12], p = 0.250; slope: 95% CI [-0.36, 0.02], p = 0.085) nor age (intercept: 95% CI [-0.26, 0.28], p = 0.926; slope: 95% CI [-0.14, 0.21], p = 0.697) predicted the latent intercept or slope of CON-FC.

Discussion

In the present study, we tested whether baseline SCD predicts a decrease in CON-FC over three years and whether the decrease in CON-FC is more pronounced in older adults with relatively lower neurite density in the forceps minor (denoted as 'CON-SC', for simplicity). We used LGCM to study individual differences in CON functional and structural connectivity in a sample of healthy older adults. We found that greater SCD predicts lower CON-FC after 3 years in individuals with relatively low neurite density in the forceps minor. However, greater SCD did not directly predict lower CON-FC after three years or a greater rate of change in CON-FC over this period. Together, these results both indicate that CON-FC alterations in SCD are dependent upon the forceps minor neurite density and support the complex effect of SCD on FC.

Our main finding is that the neurite density in the forceps minor moderated the effect of SCD on CON-FC. SCD is a behavioral phenotype with multiple causes and trajectories in relation to cognitive function (Jessen et al., 2020; Rabin et al., 2017). Our finding thus indicates that one trajectory of SCD leading to functional brain changes such as decreased CON-FC depends on the neurite density of, at least, one major frontal white-matter tract, the forceps minor. This finding also implies that neurite density in the forceps minor might be a potential biomarker for functional brain changes in individuals with SCD. The functional relevance of the frontal white matter, including the genu of the corpus callosum, has been implied by the cross-sectional association between fractional anisotropy in the frontal white matter and processing speed in healthy older adults (Hong et al., 2015). Future longitudinal studies could help elucidate whether decreased visual processing speed, one of the cognitive functions supported by the CON-FC (Ruiz-Rizzo et al., 2019), depends on the neurite density in, specifically, the forceps minor in SCD.

Our analyses revealed that the neurite density of the forceps minor was negatively correlated with age, in line with previous reports for fractional anisotropy and mean diffusivity (de Groot et al., 2015) and voxelwise neurite density (Merluzzi et al., 2016). This result also helps us better understand the moderating role of CON-SC in the effect of SCD on CON-FC, found in the present study. Specifically, the effect of SCD on CON-FC appears to be stronger for older adults who are more sensitive to age effects on CON-SC. Aging is associated with a high load of white matter hyperintensities, which tend to accumulate, mostly, in the frontal lobes (Raz et al., 2007). White matter hyperintensities are indicative of small vessel disease (Wardlaw et al., 2015). Accordingly, it seems plausible that vascular risk factors or particular age-related vascular damage in frontal regions might contribute to a neurite density reduction in the forceps minor. In line with previous studies (e.g., Wang et al., 2012;

Wen et al., 2019), we observed a negative but non-significant correlation between SCD and CON-SC. Larger sample sizes or a longer follow-up period in future studies might help determine whether there indeed is a direct association between SCD and CON-SC. Regardless, our results imply that CON-SC might allow identifying individuals with SCD in whom prevention strategies (e.g., aimed at reducing vascular risk factors) may counteract functional brain decreases.

The LGCM approach used in the present study allowed us to separate the effect of the interaction between CON-SC and SCD on CON-FC at a particular time throughout the 3-year measurement period. Contrary to what was observed for the latent intercept, CON-SC did not moderate the effect of SCD on the rate of change of CON-FC (latent slope). The observed tendency was an overall decrease with greater SCD, independently of the level of neurite density in the forceps minor. In previous studies, greater SCD has been found associated with more pronounced cognitive decline in memory functions across follow-ups spanning substantially larger follow-up periods, i.e., ~11 years (Hohman et al., 2011). Similarly, rates of cognitive decline have been shown to differ between older adults with and without SCD only after 6 years from baseline (Koppara et al., 2015). Accordingly, and assuming a similar effect for FC, a measurement period > 3 years might help ascertain whether CON-SC does also modulate the rate of decrease of CON-FC. Overall, our results suggest that CON-SC is relevant for the prediction of the level of CON-FC after three years, in individuals with the subjective impression of decline in their cognitive functions.

Our results should be interpreted taking some limitations into account. For example, our sample size is small for LGCM approaches, which work best with sample sizes ≥ 100 (e.g., Curran et al., 2010). Nevertheless, our study can set the ground for future longitudinal studies that combine FC and SC measures in a theory-driven manner in the context of SCD. Additionally, both MRI-based functional and

structural connectivity are indirect measures of connectivity. Despite this limitation, our study showed that combining both can offer a more comprehensive understanding of the changes in brain organization that might occur with SCD. Depressive symptoms and conscientiousness scores increased with SCD and time in our sample, thereby raising the possibility that they can partly explain the associations found between SCD and brain connectivity. However, subclinical depressive symptoms (i.e., a score < 5 on the GDS; Bijl et al., 2006) and particular personality factors (such as high neuroticism or conscientiousness) often co-occur with SCD and might either result from SCD or share the same underlying cause as SCD (Jenkins et al., 2019; Jessen et al., 2020). Finally, averaging CON-SC across all time points required making assumptions that could not be directly tested in the present study (e.g., measurement invariance, interchangeability of observations, and interpretation of the average) but that merit a deeper investigation in the future.

To conclude, we found that SCD predicts lower CON-FC over three years in individuals with relatively lower neurite density of the forceps minor, a major frontal white-matter tract. Advanced age can have an impact on the neurite density of the forceps minor. Together, these findings imply modifiable age-related factors that could help delay or mitigate both age and SCD-related effects on brain connectivity.

Acknowledgments

This work was supported by the European Union's Framework Programme for Research and Innovation Horizon 2020 (2014-2020) [Marie Skłodowska-Curie Grant Agreement No. 754388 (LMUResearchFellows)]; LMUexcellent [funded by the Federal Ministry of Education and Research (BMBF) and the Free State of Bavaria under the Excellence Strategy of the German Federal Government and the Länder]; and the Netherlands Organisation for Scientific Research [Veni grant: 016.136.072]

CRediT author contribution

A.R.: Conceptualization, Data curation, Formal analysis, Methodology, Software, Visualization, Writing – original draft, Writing – review & editing; R.V.: Data curation, Formal analysis, Investigation, Resources, Software, Writing – review & editing; A.D.: Methodology, Writing – review & editing; K.F.: Supervision, Writing – review & editing; H.M.: Supervision, Writing – review & editing; J.D.: Conceptualization, Funding acquisition, Methodology, Supervision, Writing – review & editing.

Conflicts of Interest

None

References

Abe, O., Masutani, Y., Aoki, S., Yamasue, H., Yamada, H., Kasai, K., Mori, H., Hayashi, N., Masumoto, T., & Ohtomo, K. (2004). Topography of the Human Corpus Callosum Using Diffusion Tensor Tractography. *Journal of Computer Assisted Tomography*, *28*(4), 533–539.

Araque Caballero, M. Á., Suárez-Calvet, M., Duering, M., Franzmeier, N., Benzinger, T., Fagan, A. M., Bateman, R. J., Jack, C. R., Levin, J., Dichgans, M., Jucker, M., Karch, C., Masters, C. L., Morris, J. C., Weiner, M., Rossor, M., Fox, N. C., Lee, J.-H., Salloway, S., … Ewers, M. (2018). White matter diffusion alterations precede symptom onset in autosomal dominant Alzheimer's disease. *Brain*, *141*(10), 3065–3080. https://doi.org/10.1093/brain/awy229

Assaf, Y., Johansen-Berg, H., & Thiebaut de Schotten, M. (2019). The role of diffusion MRI in neuroscience. *NMR in Biomedicine*, *32*(4), e3762. https://doi.org/10.1002/nbm.3762

Behrens, T. E. J., Berg, H. J., Jbabdi, S., Rushworth, M. F. S., & Woolrich, M. W. (2007). Probabilistic diffusion tractography with multiple fibre orientations: What can we gain? *NeuroImage*, *34*(1), 144–155. https://doi.org/10.1016/j.neuroimage.2006.09.018

Bijl, D., van Marwijk, H. WJ., Adér, H. J., Beekman, A. T. F., & de Haan, M. (2006). Test-Characteristics of the GDS-15 in Screening for Major Depression in Elderly Patients in General Practice. *Clinical Gerontologist*, *29*(1), 1–9. https://doi.org/10.1300/J018v29n01_01

Bollen, K. A., & Noble, M. D. (2011). Structural equation models and the quantification of behavior. *Proceedings of the National Academy of Sciences*, *108*(supplement_3), 15639–15646. https://doi.org/10.1073/pnas.1010661108

Curran, P. J., Obeidat, K., & Losardo, D. (2010). Twelve Frequently Asked Questions About Growth Curve Modeling. *Journal of Cognition and Development*, *11*(2), 121–136. https://doi.org/10.1080/15248371003699969

Daducci, A., Canales-Rodríguez, E. J., Zhang, H., Dyrby, T. B., Alexander, D. C., & Thiran, J.-P. (2015). Accelerated Microstructure Imaging via Convex Optimization (AMICO) from diffusion MRI data. *NeuroImage*, *105*, 32–44. https://doi.org/10.1016/j.neuroimage.2014.10.026

Daugherty, A. M., & Raz, N. (2016). Accumulation of iron in the putamen predicts its shrinkage in healthy older adults: A multi-occasion longitudinal study. *NeuroImage*, *128*, 11–20. https://doi.org/10.1016/j.neuroimage.2015.12.045

de Groot, M., Ikram, M. A., Akoudad, S., Krestin, G. P., Hofman, A., van der Lugt, A., Niessen, W. J., & Vernooij, M. W. (2015). Tract-specific white matter degeneration in aging: The Rotterdam Study. *Alzheimer's & Dementia*, *11*(3), 321–330. https://doi.org/10.1016/j.jalz.2014.06.011

Dosenbach, N. U. F., Fair, D. A., Miezin, F. M., Cohen, A. L., Wenger, K. K.,

Dosenbach, R. A. T., Fox, M. D., Snyder, A. Z., Vincent, J. L., Raichle, M. E., Schlaggar, B. L., & Petersen, S. E. (2007). Distinct brain networks for adaptive and stable task control in humans. *Proceedings of the National Academy of Sciences*, *104*(26), 11073–11078. https://doi.org/10.1073/pnas.0704320104

Enders, C. K., & Bandalos, D. L. (2001). The Relative Performance of Full Information Maximum Likelihood Estimation for Missing Data in Structural Equation Models. *Structural Equation Modeling: A Multidisciplinary Journal*, *8*(3), 430–457. https://doi.org/10.1207/S15328007SEM0803_5

Figley, T. D., Bhullar, N., Courtney, S. M., & Figley, C. R. (2015). Probabilistic atlases of default mode, executive control and salience network white matter tracts: An fMRI-guided diffusion tensor imaging and tractography study. *Frontiers in Human Neuroscience*, *9*. https://doi.org/10.3389/fnhum.2015.00585

Fischl, B. (2012). FreeSurfer. *NeuroImage*, *62*(2), 774–781. https://doi.org/10.1016/j.neuroimage.2012.01.021

Folstein, M. F., Folstein, S. E., & McHugh, P. R. (1975). “Mini-mental state”: A practical method for grading the cognitive state of patients for the clinician. *Journal of Psychiatric Research*, *12*(3), 189–198. https://doi.org/10.1016/0022-3956(75)90026-6

Friston, K. J. (1994). Functional and effective connectivity in neuroimaging: A synthesis. *Human Brain Mapping*, *2*(1–2), 56–78. https://doi.org/10.1002/hbm.460020107

Gilewski, M. J., Zelinski, E. M., & Schaie, K. W. (1990). The Memory Functioning Questionnaire for assessment of memory complaints in adulthood and old age. *Psychology and Aging*, *5*(4), 482–490. https://doi.org/10.1037/0882-7974.5.4.482

Glasser, M. F., Coalson, T. S., Robinson, E. C., Hacker, C. D., Harwell, J., Yacoub, E.,

Ugurbil, K., Andersson, J., Beckmann, C. F., Jenkinson, M., Smith, S. M., & Van Essen, D. C. (2016). A multi-modal parcellation of human cerebral cortex. *Nature*, *536*(7615), 171–178. https://doi.org/10.1038/nature18933

He, X., Qin, W., Liu, Y., Zhang, X., Duan, Y., Song, J., Li, K., Jiang, T., & Yu, C. (2014). Abnormal salience network in normal aging and in amnestic mild cognitive impairment and Alzheimer's disease. *Human Brain Mapping*, *35*(7), 3446–3464. https://doi.org/10.1002/hbm.22414

Hohman, T. J., Beason-Held, L. L., Lamar, M., & Resnick, S. M. (2011). Subjective cognitive complaints and longitudinal changes in memory and brain function. *Neuropsychology*, *25*(1), 125–130. https://doi.org/10.1037/a0020859

Honey, C. J., Sporns, O., Cammoun, L., Gigandet, X., Thiran, J. P., Meuli, R., & Hagmann, P. (2009). Predicting human resting-state functional connectivity from structural connectivity. *Proceedings of the National Academy of Sciences*, *106*(6), 2035–2040. https://doi.org/10.1073/pnas.0811168106

Hong, Z., Ng, K. K., Sim, S. K. Y., Ngeow, M. Y., Zheng, H., Lo, J. C., Chee, M. W. L., & Zhou, J. (2015). Differential age-dependent associations of gray matter volume and white matter integrity with processing speed in healthy older adults. *NeuroImage*, *123*, 42–50. https://doi.org/10.1016/j.neuroimage.2015.08.034

Jenkins, A., Tree, J. J., Thornton, I. M., & Tales, A. (2019). Subjective Cognitive Impairment in 55-65-Year-Old Adults Is Associated with Negative Affective Symptoms, Neuroticism, and Poor Quality of Life. *Journal of Alzheimer's Disease*, *67*(4), 1367–1378. https://doi.org/10.3233/JAD-180810

Jenkinson, M., Bannister, P., Brady, M., & Smith, S. (2002). Improved Optimization for the Robust and Accurate Linear Registration and Motion Correction of Brain Images. *NeuroImage*, *17*(2), 825–841. https://doi.org/10.1006/nimg.2002.1132

Jenkinson, M., Beckmann, C. F., Behrens, T. E. J., Woolrich, M. W., & Smith, S. M.

(2012). FSL. *NeuroImage*, *62*(2), 782–790. https://doi.org/10.1016/j.neuroimage.2011.09.015

Jessen, F., Amariglio, R. E., Buckley, R. F., van der Flier, W. M., Han, Y., Molinuevo, J. L., Rabin, L., Rentz, D. M., Rodriguez-Gomez, O., Saykin, A. J., Sikkes, S. A. M., Smart, C. M., Wolfsgruber, S., & Wagner, M. (2020). The characterisation of subjective cognitive decline. *The Lancet Neurology*, *19*(3), 271–278. https://doi.org/10.1016/S1474-4422(19)30368-0

John, O. P., Donahue, E. M., & Kentle, R. L. (1991). *The Big Five Inventory—Versions 4a and 54*. University of California, Berkeley; Institute of Personality and Social Research, Berkeley, CA. https://www.ocf.berkeley.edu/~johnlab/bfi.htm

Koppara, A., Wagner, M., Lange, C., Ernst, A., Wiese, B., König, H.-H., Brettschneider, C., Riedel-Heller, S., Luppa, M., Weyerer, S., Werle, J., Bickel, H., Mösch, E., Pentzek, M., Fuchs, A., Wolfsgruber, S., Beauducel, A., Scherer, M., Maier, W., & Jessen, F. (2015). Cognitive performance before and after the onset of subjective cognitive decline in old age. *Alzheimer's & Dementia: Diagnosis, Assessment & Disease Monitoring*, *1*(2), 194–205. https://doi.org/10.1016/j.dadm.2015.02.005

La Joie, R., Perrotin, A., Egret, S., Pasquier, F., Tomadesso, C., Mézenge, F., Desgranges, B., de La Sayette, V., & Chételat, G. (2016). Qualitative and quantitative assessment of self-reported cognitive difficulties in nondemented elders: Association with medical help seeking, cognitive deficits, and β-amyloid imaging. *Alzheimer's & Dementia: Diagnosis, Assessment & Disease Monitoring*, *5*, 23–34. https://doi.org/10.1016/j.dadm.2016.12.005

Little, R. J. A. (1988). A Test of Missing Completely at Random for Multivariate Data with Missing Values. *Journal of the American Statistical Association*, *83*(404), 1198–1202. https://doi.org/10.1080/01621459.1988.10478722

Little, T. D., Jorgensen, T. D., Lang, K. M., & Moore, E. W. G. (2014). On the Joys of Missing Data. *Journal of Pediatric Psychology*, *39*(2), 151–162. https://doi.org/10.1093/jpepsy/jst048

Luo, C., Li, M., Qin, R., Chen, H., Yang, D., Huang, L., Liu, R., Xu, Y., Bai, F., & Zhao, H. (2020). White Matter Microstructural Damage as an Early Sign of Subjective Cognitive Decline. *Frontiers in Aging Neuroscience*, *11*. https://www.frontiersin.org/article/10.3389/fnagi.2019.00378

McArdle, J. J. (2009). Latent variable modeling of differences and changes with longitudinal data. *Annual Review of Psychology*, *60*, 577–605. https://doi.org/10.1146/annurev.psych.60.110707.163612

McAvinue, L. P., Habekost, T., Johnson, K. A., Kyllingsbæk, S., Vangkilde, S., Bundesen, C., & Robertson, I. H. (2012). Sustained attention, attentional selectivity, and attentional capacity across the lifespan. *Attention, Perception, & Psychophysics*, *74*(8), 1570–1582. https://doi.org/10.3758/s13414-012-0352-6

Merluzzi, A. P., Dean, D. C., Adluru, N., Suryawanshi, G. S., Okonkwo, O. C., Oh, J. M., Hermann, B. P., Sager, M. A., Asthana, S., Zhang, H., Johnson, S. C., Alexander, A. L., & Bendlin, B. B. (2016). Age-dependent differences in brain tissue microstructure assessed with neurite orientation dispersion and density imaging. *Neurobiology of Aging*, *43*, 79–88. https://doi.org/10.1016/j.neurobiolaging.2016.03.026

Molinuevo, J. L., Rabin, L. A., Amariglio, R., Buckley, R., Dubois, B., Ellis, K. A., Ewers, M., Hampel, H., Klöppel, S., Rami, L., Reisberg, B., Saykin, A. J., Sikkes, S., Smart, C. M., Snitz, B. E., Sperling, R., van der Flier, W. M., Wagner, M., & Jessen, F. (2017). Implementation of subjective cognitive decline criteria in research studies. *Alzheimer's & Dementia*, *13*(3), 296–311. https://doi.org/10.1016/j.jalz.2016.09.012

Ohlhauser, L., Parker, A. F., Smart, C. M., & Gawryluk, J. R. (2019). White matter and its relationship with cognition in subjective cognitive decline. *Alzheimer's & Dementia: Diagnosis, Assessment & Disease Monitoring*, *11*, 28–35. https://doi.org/10.1016/j.dadm.2018.10.008

Onoda, K., Ishihara, M., & Yamaguchi, S. (2012). Decreased Functional Connectivity by Aging Is Associated with Cognitive Decline. *Journal of Cognitive Neuroscience*, *24*(11), 2186–2198. https://doi.org/10.1162/jocn_a_00269

Pruim, R. H. R., Mennes, M., van Rooij, D., Llera, A., Buitelaar, J. K., & Beckmann, C. F. (2015). ICA-AROMA: A robust ICA-based strategy for removing motion artifacts from fMRI data. *NeuroImage*, *112*, 267–277. https://doi.org/10.1016/j.neuroimage.2015.02.064

R Core Team. (2021). *R: The R Project for Statistical Computing*. https://www.r-project.org/

Rabin, L. A., Smart, C. M., & Amariglio, R. E. (2017). Subjective cognitive decline in preclinical Alzheimer's disease. *Annual Review of Clinical Psychology*, *13*, 369–396. https://doi.org/10.1146/annurev-clinpsy-032816-045136

Raichle, M. E. (2015). The restless brain: How intrinsic activity organizes brain function. *Philosophical Transactions of the Royal Society B: Biological Sciences*, *370*(1668), 20140172. https://doi.org/10.1098/rstb.2014.0172

Raz, N., Rodrigue, K. M., Kennedy, K. M., & Acker, J. D. (2007). Vascular health and longitudinal changes in brain and cognition in middle-aged and older adults. *Neuropsychology*, *21*(2), 149–157. https://doi.org/10.1037/0894-4105.21.2.149

Reitan, R. M., & Wolfson, D. (1986). The Halstead-Reitan Neuropsychological Test Battery. In *The neuropsychology handbook: Behavioral and clinical perspectives* (pp. 134–160). Springer Publishing Co.

Rey, A. (1958). *L'examen clinique en psychologie. [The clinical examination in*

psychology.] (p. 222). Presses Universitaries De France.

Rosseel, Y. (2012). lavaan: An R Package for Structural Equation Modeling. *Journal of Statistical Software*, *48*, 1–36. https://doi.org/10.18637/jss.v048.i02

RStudio Team. (2021). *RStudio: Integrated Development Environment for R* (1.4.1717) [Computer software]. https://rstudio.com/

Ruiz-Rizzo, A. L., Neitzel, J., Müller, H. J., Sorg, C., & Finke, K. (2018). Distinctive Correspondence Between Separable Visual Attention Functions and Intrinsic Brain Networks. *Frontiers in Human Neuroscience*, *12*. https://doi.org/10.3389/fnhum.2018.00089

Ruiz-Rizzo, A. L., Sorg, C., Napiórkowski, N., Neitzel, J., Menegaux, A., Müller, H. J., Vangkilde, S., & Finke, K. (2019). Decreased cingulo-opercular network functional connectivity mediates the impact of aging on visual processing speed. *Neurobiology of Aging*, *73*, 50–60. https://doi.org/10.1016/j.neurobiolaging.2018.09.014

Sadaghiani, S., & Kleinschmidt, A. (2016). Brain Networks and α-Oscillations: Structural and Functional Foundations of Cognitive Control. *Trends in Cognitive Sciences*, *20*(11), 805–817. https://doi.org/10.1016/j.tics.2016.09.004

Schreiber, J. B., Nora, A., Stage, F. K., Barlow, E. A., & King, J. (2006). Reporting Structural Equation Modeling and Confirmatory Factor Analysis Results: A Review. *The Journal of Educational Research*, *99*(6), 323–338. https://doi.org/10.3200/JOER.99.6.323-338

Smith, S. M. (2002). Fast robust automated brain extraction. *Human Brain Mapping*, *17*(3), 143–155. https://doi.org/10.1002/hbm.10062

Smith, S. M., Jenkinson, M., Woolrich, M. W., Beckmann, C. F., Behrens, T. E. J., Johansen-Berg, H., Bannister, P. R., De Luca, M., Drobnjak, I., Flitney, D. E., Niazy, R. K., Saunders, J., Vickers, J., Zhang, Y., De Stefano, N., Brady, J. M.,

& Matthews, P. M. (2004). Advances in functional and structural MR image analysis and implementation as FSL. *NeuroImage*, *23*, S208–S219. https://doi.org/10.1016/j.neuroimage.2004.07.051

Stroop, J. R. (1935). Studies of interference in serial verbal reactions. *Journal of Experimental Psychology*, *18*(6), 643–662. https://doi.org/10.1037/h0054651

Tu, M.-C., Lo, C.-P., Huang, C.-F., Huang, W.-H., Deng, J. F., & Hsu, Y.-H. (2018). Visual Attention Performances and Related Cerebral Microstructural Integrity Among Subjects With Subjective Cognitive Decline and Mild Cognitive Impairment. *Frontiers in Aging Neuroscience*, *10*. https://www.frontiersin.org/article/10.3389/fnagi.2018.00268

Valech, N., Tort-Merino, A., Coll-Padrós, N., Olives, J., León, M., Rami, L., & Molinuevo, J. L. (2018). Executive and Language Subjective Cognitive Decline Complaints Discriminate Preclinical Alzheimer's Disease from Normal Aging. *Journal of Alzheimer's Disease*, *61*(2), 689–703. https://doi.org/10.3233/JAD-170627

van de Schoot, R., Lugtig, P., & Hox, J. (2012). A checklist for testing measurement invariance. *European Journal of Developmental Psychology*, *9*(4), 486–492. https://doi.org/10.1080/17405629.2012.686740

Viviano, R. P., & Damoiseaux, J. S. (2020). Functional neuroimaging in subjective cognitive decline: Current status and a research path forward. *Alzheimer's Research & Therapy*, *12*(1), 23. https://doi.org/10.1186/s13195-020-00591-9

Viviano, R. P., & Damoiseaux, J. S. (2021). Longitudinal change in hippocampal and dorsal anterior insulae functional connectivity in subjective cognitive decline. *Alzheimer's Research & Therapy*, *13*(1), 108. https://doi.org/10.1186/s13195-021-00847-y

Viviano, R. P., Hayes, J. M., Pruitt, P. J., Fernandez, Z. J., van Rooden, S., van der

Grond, J., Rombouts, S. A. R. B., & Damoiseaux, J. S. (2019). Aberrant memory system connectivity and working memory performance in subjective cognitive decline. *NeuroImage*, *185*, 556–564. https://doi.org/10.1016/j.neuroimage.2018.10.015

Wakana, S., Jiang, H., Nagae-Poetscher, L. M., van Zijl, P. C. M., & Mori, S. (2004). Fiber Tract–based Atlas of Human White Matter Anatomy. *Radiology*, *230*(1), 77–87. https://doi.org/10.1148/radiol.2301021640

Wang, Y., West, J. D., Flashman, L. A., Wishart, H. A., Santulli, R. B., Rabin, L. A., Pare, N., Arfanakis, K., & Saykin, A. J. (2012). Selective changes in white matter integrity in MCI and older adults with cognitive complaints. *Biochimica et Biophysica Acta (BBA) - Molecular Basis of Disease*, *1822*(3), 423–430. https://doi.org/10.1016/j.bbadis.2011.08.002

Wang, Z., Dai, Z., Gong, G., Zhou, C., & He, Y. (2015). Understanding Structural-Functional Relationships in the Human Brain: A Large-Scale Network Perspective. *The Neuroscientist*, *21*(3), 290–305. https://doi.org/10.1177/1073858414537560

Wardlaw, J. M., Valdés Hernández, M. C., & Muñoz-Maniega, S. (2015). What are White Matter Hyperintensities Made of? *Journal of the American Heart Association: Cardiovascular and Cerebrovascular Disease*, *4*(6), e001140. https://doi.org/10.1161/JAHA.114.001140

Wechsler, D. (1997). *Wechsler Adult Intelligence Scale* | *Third Edition*. Pearson Assessments.

Wechsler, D. (2009). *Wechsler Memory Scale* | *Fourth Edition*.

Wechsler, D. (2011). *Wechsler Abbreviated Scale of Intelligence* | *Second Edition*.

Wen, Q., Mustafi, S. M., Li, J., Risacher, S. L., Tallman, E., Brown, S. A., West, J. D., Harezlak, J., Farlow, M. R., Unverzagt, F. W., Gao, S., Apostolova, L. G.,

Saykin, A. J., & Wu, Y.-C. (2019). White matter alterations in early-stage Alzheimer's disease: A tract-specific study. *Alzheimer's & Dementia: Diagnosis, Assessment & Disease Monitoring*, *11*, 576–587. https://doi.org/10.1016/j.dadm.2019.06.003

Woolrich, M. W., Ripley, B. D., Brady, M., & Smith, S. M. (2001). Temporal Autocorrelation in Univariate Linear Modeling of FMRI Data. *NeuroImage*, *14*(6), 1370–1386. https://doi.org/10.1006/nimg.2001.0931

Yendiki, A., Panneck, P., Srinivasan, P., Stevens, A., Zöllei, L., Augustinack, J., Wang, R., Salat, D., Ehrlich, S., Behrens, T., Jbabdi, S., Gollub, R., & Fischl, B. (2011). Automated Probabilistic Reconstruction of White-Matter Pathways in Health and Disease Using an Atlas of the Underlying Anatomy. *Frontiers in Neuroinformatics*, *5*. https://www.frontiersin.org/article/10.3389/fninf.2011.00023

Yesavage, J. A., Brink, T. L., Rose, T. L., Lum, O., Huang, V., Adey, M., & Leirer, V. O. (1982). Development and validation of a geriatric depression screening scale: A preliminary report. *Journal of Psychiatric Research*, *17*(1), 37–49. https://doi.org/10.1016/0022-3956(82)90033-4

Zhang, H., Schneider, T., Wheeler-Kingshott, C. A., & Alexander, D. C. (2012). NODDI: Practical in vivo neurite orientation dispersion and density imaging of the human brain. *NeuroImage*, *61*(4), 1000–1016. https://doi.org/10.1016/j.neuroimage.2012.03.072